Appl Phys A (2008) 92: 505–510
DOI 10.1007/s00339-008-4550-y

Applied Physics A
Materials Science & Processing

Domain wall dynamics and interlayer interactions in magnetic trilayer systems studied by XMCD-PEEM

J. Vogel · W. Kuch · K. Fukumoto · F. Romanens · S. Pizzini · J. Camarero

Received: 9 October 2007 / Accepted: 3 April 2008 / Published online: 16 May 2008

Abstract We have used time-resolved x-ray magnetic circular dichroism combined with photoemission electron microscopy (XMCD-PEEM) to investigate the layer-resolved microscopic magnetization reversal in FeNi/X/Co (with X = Cu, Al_2O_3) trilayer systems. These measurements were performed in pump-probe mode, synchronizing magnetic pulses with synchrotron x-ray pulses. The good magnetic contrast observed for most samples reveals that in many cases the magnetization reversal is reproducible. We have used the measurements to obtain domain wall propagation speeds as a function of applied magnetic field, and to investigate the influence of domain wall interactions on the magnetic switching.

PACS 07.85.Qe · 75.60.Ch · 75.60.Jk · 75.70.Ak · 85.70.Kh

J. Vogel (✉) · F. Romanens · S. Pizzini
Institut Néel, CNRS-UJF, 25 rue des martyrs, 38000 Grenoble, France
e-mail: jan.vogel@grenoble.cnrs.fr

W. Kuch · K. Fukumoto
Institut für Experimentalphysik, Freie Universität Berlin, Arnimallee 14, 14195 Berlin, Germany

Present address:
K. Fukumoto
SPring-8, 1-1-1 Kouto, Sayo-cho, Sayo-gun, Hyogo 679-5198, Japan

J. Camarero
Departmento Física de la Materia Condensada, Universidad Autónoma de Madrid, 28049 Madrid, Spain

1 Introduction

Many devices used in magnetic storage, like Magnetic Tunnel Junctions (MTJ) and Spin Valves (SV) rely on the giant magnetoresistance effect [1, 2], the dependence of the resistance of a multilayered magnetic system on the relative orientation of the magnetization directions in different magnetic layers separated by nonmagnetic spacer layers. The interplay between electron currents and local magnetization through the electron spins can also lead to the inverse effect, the switching of magnetization by a spin-polarized current, as has been shown recently [3, 4]. In both cases, it is important to get microscopic information on the switching of each magnetic layer separately, and on the interaction between the magnetic layers through the nonmagnetic spacer layers. This information can be obtained by combing the element selectivity of time-resolved x-ray Magnetic Circular Dichroism (XMCD) [5] with the spatial resolution of Photoemission Electron Microscopy (PEEM) [6–8]. The first time-resolved XMCD-PEEM results were published in 2003 [9, 10], and the technique has since then been used mainly for studying magnetization dynamics in soft magnetic permalloy microstructures [11–14] and in FeNi/X/Co (with $X = \mathrm{Cu}, \mathrm{Al_2O_3}$) trilayer systems [9, 15–20]. It has enabled obtaining detailed information on the dynamics of magnetic domains, domain walls and vortices in flux-closure magnetic patterns [11–14], on domain wall propagation speeds in continuous films [18] and on the influence of magnetic anisotropy [16], domain wall interactions [17] and layer topography [19] on the switching of the soft magnetic layer in trilayer systems. In this paper we review some of the results we obtained on trilayer systems at the BESSY synchrotron.

2 Experimental details

All of the above-mentioned experiments were performed in a pump-probe or stroboscopic mode, in which the system was excited using magnetic pulses that were synchronized with synchrotron x-ray pulses [5]. In our case, the measurements were performed at the BESSY synchrotron in Berlin (Germany), on beamlines UE56/2-PGM2 and UE52-SGM. The synchrotron was operated in the single-bunch mode, with one single bunch of electrons in the storage ring, giving rise to x-ray photon pulses with a repetition rate of 1.25 MHz and a bunch length of about 50–70 ps. Magnetic pulses were applied to the sample at half (625 kHz) or one-quarter (312.5 kHz) of this repetition rate, to limit power dissipation in the pulsed current supply. Details of the experimental setup were given in [9] and [20]. With this system, bipolar magnetic pulses with amplitudes up to 15 mT and pulse durations of several tens of nanoseconds could be applied at repetition rates up to 625 kHz.

3 Experimental results

3.1 Reproducibility

Since one single bunch of x-ray photons does not generate a sufficient number of secondary electrons to create an image of the sample surface, images have to be accumulated over several tens of millions of photon pulses. An identical magnetic pulse has to be associated to each of the photon pulses, with a well defined delay between photon and magnetic pulses. Using this pump-probe technique, the magnetization reversal induced by each magnetic pulse has therefore to be reversible and reproducible in order to obtain good magnetic contrast in the images. In general, the reversible behavior is obtained by using a soft magnetic microstructure with an equilibrium, demagnetized multidomain state (like a Landau pattern) at zero applied magnetic field [11–14]. After the magnetic excitation pulse, the domain structure will go back to this equilibrium state if the time between two magnetic pulses is sufficiently long. For the continuous layers with in-plane magnetization that we have studied this kind of equilibrium multidomain structure does in general not exist. As the initial, reversible magnetization state in our measurements we use thus either a saturated, single domain state, or a domain state that is imposed by a magnetic coupling between the FeNi and Co layers through the nonmagnetic interlayer. In the latter case, the sample was first demagnetized to obtain a multidomain state, and the nanosecond switching was then studied for magnetic pulses with an amplitude sufficient to reverse the (soft magnetic) FeNi layer without changing the domain state in the (magnetically harder) Co layer. The Co domain state acts then, through the coupling, as a 'template' for the zero-field domain state of the FeNi layer.

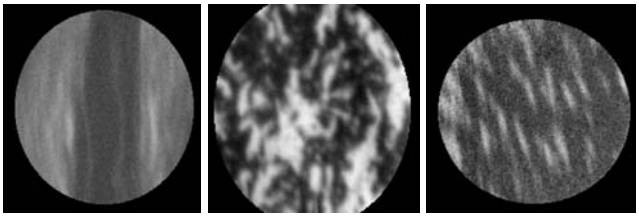

Fig. 1 Stroboscopic magnetic domain images of the FeNi layer of different FeNi/X/Co trilayers observed using XMCD-PEEM at the Fe L_3-edge *during* magnetic field pulses of about 3–5 mT. (**a**) FeNi(5 nm)/Cu(4 nm)/Co(8 nm) on Si(001), presenting an in-plane uniaxial anisotropy with the easy axis vertical in the image. (**b**) FeNi(5 nm)/Cu(4 nm)/Co(5 nm) on Si(001), presenting no clear anisotropy axis within the plane of the layers. (**c**) FeNi(4 nm)/Al_2O_3(2.6 nm)/Co(8 nm) on step-bunched Si(111), miscut by 6° along the $(\bar{2}11)$ direction, presenting a strong uniaxial magnetic anisotropy with the easy axis vertical in the image. The field of view is about 100 μm for images (**a**) and (**c**), and about 30 μm for image (**b**)

In extended or continuous films, magnetization reversal takes place by nucleation of domains and propagation of domain walls. These processes are thermally assisted, inducing some nonreproducibility in the magnetization reversal. In high-quality magnetic garnet films, for example, magnetic defects are rare and nucleation of reversed magnetic domains, starting from a saturated state, can take place with almost equal probability on any site of the sample [21]. However, once nucleated the domain walls will propagate with a speed determined only by the magnetic field. In pump-probe experiments on this type of materials, homogeneous grey images will thus be obtained if starting from a saturated state before each reversal. However, if domains are not completely annihilated in between pulses, and only domain wall motion takes place during the pulse, images with a good magnetic contrast will be obtained.

We have studied FeNi/X/Co trilayer systems deposited on different substrates and using different deposition conditions. Examples of stroboscopic domain images obtained during magnetic field pulses on different systems are shown in Fig. 1. The samples were $Fe_{20}Ni_{80}$(5 nm)/Cu(4 nm)/Co(8 nm) deposited on flat Si(001) under magnetic field (sample 1, Fig. 1a), $Fe_{20}Ni_{80}$(5 nm) /Cu(4 nm) /Co(5 nm) on flat Si(001) deposited without applied magnetic field (sample 2, Fig. 1b), and $Fe_{20}Ni_{80}$(5 nm)/Al_2O_3 (2.6 nm)/Co(8 nm) on step-bunched Si(111) (sample 3, Fig. 1c). The images were obtained at the Fe L_3 edge, showing the domain structure during reversal of the FeNi layer only. The image of Fig. 1a shows rather weak contrast, with several shades of grey. In this sample, the deposition under applied magnetic field was at the origin of a small uniaxial in-plane magnetic anisotropy, with the easy magnetization axis being

vertical in the images. For this reason, some elongated vertical structures can be seen, since the anisotropy favors domains elongated in this direction. However, the weak contrast of this image indicates that both nucleation and domain wall propagation are not very reproducible in this sample. In the Stoner–Wohlfarth model [22], the field necessary for magnetization reversal is proportional to the magnetic anisotropy. This model is also frequently used for nucleation of reversed domains in continuous films [23], indicating that the nucleation barriers are quite small in this sample due to the small anisotropy. In that case, several nucleation sites with almost equivalent energy barriers are expected to exist on the sample, which are activated randomly during the different magnetic pulses. The nonreproducibility of the propagation of domain walls can be explained by the stiffness of the domain walls due to the anisotropy, leading to propagation by non-reproducible, thermally activated Barkhausen jumps [16].

Sample 2 (Fig. 1b) was very similar to sample 1, the main difference being the absence of a clear magnetic anisotropy within the plane of the layers. However, the domain structure and magnetic contrast during reversal are very different for this sample. The absence of a preferential direction for the magnetization within the plane leads to irregularly shaped domains and a high density of domain walls. This favors the creation of 360° domain walls during the initial magnetic pulses, which are then not completely annihilated during subsequent pulses [20]. The observed dynamics after the initial pulses then corresponds to the expansion and compression of these 360° Néel domain walls. Due to their deformability the domain walls are easily pinned and their propagation takes place by small jumps from one pinning center to the next, which is much more reproducible than the Barkhausen jumps in the previous sample. The difference in anisotropy for these otherwise very similar samples causes therefore a large difference in dynamic behavior. Especially, the absence of nucleation of new domains and the deformability of the domain walls leads to a much more reproducible dynamic behavior for this sample without in-plane anisotropy [15, 16].

Another type of samples for which we found a reproducible dynamic behavior were trilayers deposited on step-bunched Si(111) substrates [24, 25]. The topography of the substrate, consisting of elongated terraces (∼1 μm long, 20–60 nm wide), is transmitted to the deposited trilayer structure. This leads to a quite strong uniaxial magnetic anisotropy of the layers with the easy axis parallel to the long axis of the terraces [26, 27]. The magnetic anisotropy, and therefore the domain wall stiffness, is larger than in sample 1. However, the magnetization reversal is much more reproducible than in sample 1, as can be seen from the good contrast in the image of Fig. 1c. The main difference to sample 1 is the topography of the magnetic layers, flat for sample 1 and modulated for sample 3. This modulated topography leads to a stronger in-plane uniaxial magnetic anisotropy as well as to structural and magnetic inhomogeneities of the layers. As a consequence, the intrinsic barrier for domain nucleation, governed by the magnetic anisotropy, is quite high and nucleation takes place at the inhomogeneities where the nucleation barrier is lower [23]. This leads to a wide distribution of energy barriers for nucleation, and each nucleation site is activated for a well-defined value of the magnetic field. The nucleation density, which is quite small for low field values, slowly increases with increasing field amplitude [18]. For this sample, with a miscut of 6°, the energy to nucleate domains is higher than the energy barrier for domain wall propagation [19]. For fields high enough to nucleate domains the domain wall propagation is already in a viscous regime [28]. In that regime, the domain wall propagation speed is constant for a given value of the magnetic field, and the domain wall motion is thus reproducible.

A certain degree of reproducibility of magnetization dynamics in thin films can thus be obtained either using magnetic pulses that are not sufficiently strong to completely saturate the films or by combining uniaxial magnetic anisotropy with magnetic sample inhomogeneity [29]. This last condition is not really a constraint, since most thin films used in applications are sputtered films with some degree of inhomogeneity and uniaxial magnetic anisotropy. We have observed magnetization reversal by nucleation and domain wall propagation with a good degree of reproducibility also in Co/Pt multilayers with perpendicular anisotropy, using Kerr microscopy [30].

3.2 Domain wall propagation speeds

We have used images of sample 3 at different values of the applied magnetic field to obtain information on the domain wall propagation speed as a function of magnetic field [18]. An example is given in Fig. 2 for an applied magnetic field of 6.3 mT. To diminish the effect of noise and limited contrast on the determination of the domain wall speed, we used the increase of the perimeter of the domains and a constant aspect ratio of the domain shape to evaluate the speed [18]. We found that the increase of the domain perimeter was constant as a function of time for a given field (fields from 4 to 6.8 mT), except when the domains were small. This latter effect can be explained by taking into account the important influence of the increase in domain wall energy for small domains, which opposes expansion of the domains [18]. In the field range we investigated, the domain wall speed increases linearly with applied field up to an effective field value of 5.2 mT, where it saturates at a value exceeding 2000 m/s. The effective field is determined as $H_{\mathrm{Appl}} - H_{\mathrm{Copl}}$ where H_{Appl} is the applied field and H_{Copl} is the coupling field with the Co layer of 1.2 mT, which is opposite to the applied field. The

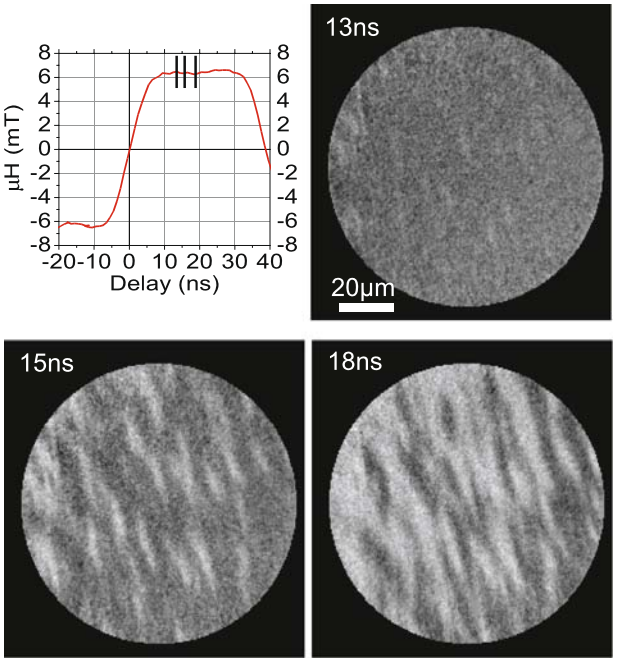

Fig. 2 Time-resolved XMCD-PEEM images of the FeNi layer of a FeNi/Al_2O_3/Co trilayer at the Fe L_3-edge during bipolar magnetic field pulses with an amplitude of 6.3 mT as shown at the top left. The images were acquired during the positive part of the pulse, with delays of 13, 15, and 18 ns between the beginning of the positive magnetic pulse and the synchrotron x-ray photon pulses. The first, negative part of the pulse was used to assure magnetic saturation in the negative (*black*) direction before each positive pulse

saturation of the domain wall propagation speed can be associated to the Walker field, the magnetic field above which changes of the internal magnetic structure take place while it is moving [31–33].

The theoretical value of the Walker breakdown field (in SI units) is given by $\frac{1}{2}\alpha J_S$, where α is the damping parameter and J_S the magnetic saturation polarization of the material. Taking often used values for permalloy of $\alpha = 0.01$ and $J_S = 1$ T, we find $H_W = 5$ mT, in excellent agreement with our experimental value. The formula for the Walker breakdown field was derived for Bloch domain walls in infinitely thick films. For thin films and nanowires, this formula has to be modified to take into account demagnetizing effects [34]. In nanowires with perpendicular anisotropy, this can lead to a reduction of the Walker field by an order of magnitude [34]. For nanowires with in-plane magnetization, a Walker breakdown field of about 1.5 mT was found for head-on domain walls [32], for a domain wall propagation speed of about 400 m/s. The fastest domain wall speeds in our experiment were found at the points of the ellipse-shaped domains, where the domain walls are also head-on. However, in our case these domain walls propagate in a continuous medium, and the strong demagnetizing fields at the borders of the nanowire in [32] are not present. In particular, the transformation during propagation of the domain wall from a transverse wall to a vortex wall and back, which takes place in the precessional regime above the Walker breakdown field [33], is not expected in our case. Part of the stray fields associated to the domain wall can also be compensated by the underlying Co layer, thus reducing the demagnetizing field [35, 36]. The homogeneous movement at low fields might therefore be stabilized up to much higher fields in the case of continuous FeNi/X/Co trilayers.

3.3 Influence of domain wall stray fields on dynamics

In the magnetic trilayer systems we have studied, the unique element-selectivity of time-resolved XMCD-PEEM can be exploited to investigate the dynamics of the two magnetic layers separately. In particular, the influence of the magnetostatic coupling between the two layers through the nonmagnetic spacer layer can be investigated. In our samples, two kinds of interactions exist. In homogeneously magnetized regions, a collinear coupling between the two layers is induced by correlated roughness at the two nonmagnetic/magnetic interfaces (the so-called Néel orange-peel coupling [37]). Close to the domain walls another type of coupling, antiparallel in this case, is induced by the domain wall stray fields [35, 36].

An example of the influence of these domain wall stray fields on the magnetization reversal dynamics is shown in Fig. 3. These images were taken for a $Fe_{20}Ni_{80}$ (5 nm)/Al_2O_3(2.6 nm)/Co(8 nm) trilayer deposited on step-bunched Si(111), miscut by 8° along the [11$\bar{2}$] direction. They were recorded at different delays between the x-ray photon pulses and the beginning of the magnetic field pulses shown in the top left panel of Fig. 3. The first ten images are taken with the x-ray photon energy tuned to the Fe L_3 absorption edge (707 eV), for the delays indicated in Fig. 3a). The last image shows the domain structure of the Co layer, recorded with the x-ray photon energy tuned to the Co L_3 edge (778 eV). This domain structure is not influenced by the magnetic field pulses. At the beginning of the pulses (delay 0 ns), the domain structure in the FeNi layer is very similar to the one in the Co layer, due to the parallel orange-peel coupling. Upon increasing field, the FeNi domain walls start moving, from the central region of the image to the right. After about 50 ns, at the end of the positive part of the bipolar field pulse, the FeNi layer is almost completely saturated in the direction of the field (black), apart from the central region where the Co domain wall is present. When the field direction changes, reversal in the white direction starts from the central region, in the vicinity of the domain wall in the Co layer. The domain wall then propagates to the right, reversing the part of the FeNi layer where external field and local coupling are parallel (white Co domains). After that, also the part of the FeNi layer above the black Co domain reverses by domain wall propagation, starting from

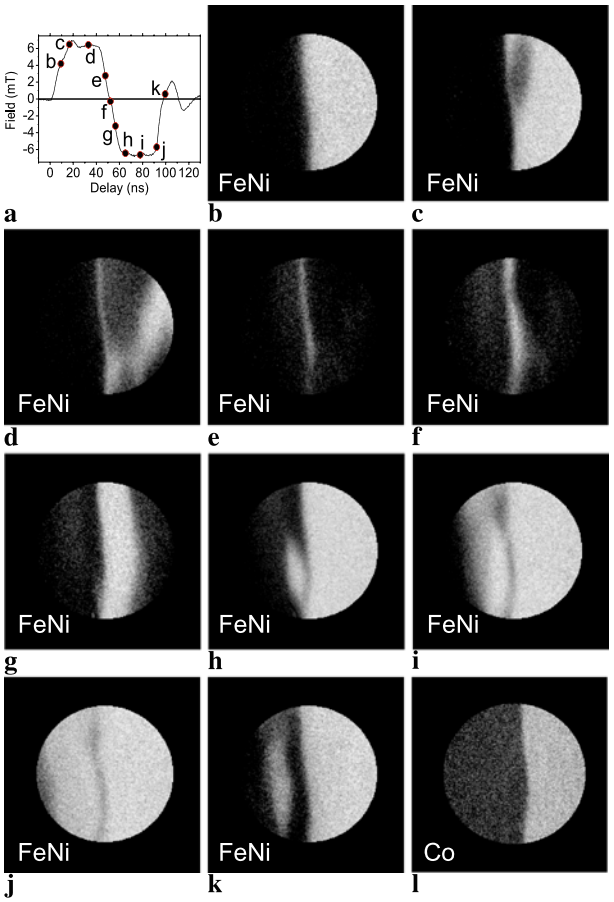

Fig. 3 Time-resolved XMCD-PEEM images for a FeNi/Al_2O_3/Co trilayer deposited on step-bunched Si(111) (8° miscut angle). (*Top left*) Temporal shape of the bipolar magnetic field pulses. The images marked FeNi are recorded with the x-ray photon energy tuned to the Fe L_3-absorption, at a delay between the beginning of the magnetic pulse and the x-ray photon pulse indicated in (**a**). The Co domain structure, which is not influenced by the magnetic field pulses, is given in the *bottom right* image. The field of view for each image is 30 µm

the quasi-wall in the center. This behavior, where reversal of the FeNi layer starts in the vicinity of domain walls in the Co layer can be explained by the Co domain wall stray fields, which tilt the FeNi magnetization away from the easy magnetization axis. This was confirmed using micromagnetic simulations performed by R. Hertel [17], showing that the stray field of Co domain walls can influence the local magnetization direction in the FeNi layer even for interlayer distances up to 100 nm. Domain wall stray fields are well known to influence the static domain configuration in trilayer systems [36, 38–42], but our measurements clearly show that also the nanosecond dynamic behavior is affected by these magnetostatic interactions. In particular, they allow a more controlled magnetization reversal by a local decrease of the energy barrier for domain nucleation.

4 Conclusions

We have used layer- and time-resolved XMCD-PEEM at the nanosecond time-scale to study the microscopic switching of the magnetization in FeNi/(Cu,Al_2O_3)/Co trilayer systems. We have developed a measurement technique that allows investigating magnetic thin films deposited on arbitrary substrates. Since the measurements are performed in a pump-probe mode, reversible and reproducible switching dynamics is necessary. Reproducible switching was obtained by either using magnetic pulses that are not sufficiently strong to completely saturate the films or by using samples with in-plane uniaxial magnetic anisotropy containing structural and magnetic inhomogeneities. We investigated the influence of interlayer coupling, magnetic anisotropy and domain wall energy on the nanosecond switching in these samples. We found that domain wall propagation speeds in the FeNi layer of these trilayer systems can exceed 2 000 m/s, much higher than in single FeNi films or nanowires. The interaction with the Co layer might stabilize the domain walls while moving. We also showed that stray fields of domain walls in the Co layer locally lead to a reduction of the barrier for nucleation of reversed domains in the FeNi layer, increasing the local switching speed.

The increase in spatial resolution of XMCD-PEEM down to below 10 nm, which can be obtained using optics for aberration corrections [43], and the upcoming availability of x-ray free electron lasers allowing a temporal resolution below 1 ps, will allow obtaining information on magnetization dynamics with unprecedented detail.

Acknowledgements We acknowledge the important contribution of M. Bonfim who made the pulsed current supplies and developed the microcoil system. We are grateful to F. Petroff, A. Vaurès and Y. Conraux for sample preparation, and to R. Hertel for micromagnetic simulations. We thank F. Helbig, B. Zada, W. Mahler, and G. Meyer for technical support. Financial support by EU (BESSY-EC-HPRI contract No. HPRI-1999-CT-00028) and the Laboratoire Européen Associé "Mesomag" is gratefully acknowledged. J.C., F.R. and J.V. acknowledge partial financial support for personnel exchange by the "Acciones Integradas-Picasso" Programme, through Grant No. HF2003-0173.

References

1. M. Baibich, J. Broto, A. Fert, F. Nguyen Van Dau, F. Petroff, P. Etienne, G. Creuzet, A. Friederich, J. Chazelas, Phys. Rev. Lett. **61**, 2472 (1988)
2. G. Binasch, P. Grünberg, F. Saurenbach, W. Zinn, Phys. Rev. B **39**, 4828 (1989)
3. J. Slonczewski, J. Magn. Magn. Mater. **159**, L1 (1996)
4. E. Myers, D. Ralph, J. Katine, R. Louie, R. Buhrman, Science **285**, 867 (1999)
5. M. Bonfim, G. Ghiringhelli, F. Montaigne, S. Pizzini, N. Brookes, F. Petroff, J. Vogel, J. Camarero, A. Fontaine, Phys. Rev. Lett. **86**, 3646 (2001)

6. J. Stöhr, Y. Wu, B. Hermsmeier, M. Samant, G. Harp, S. Koranda, D. Dunham, B. Tonner, Science **259**, 658 (1993)
7. C. Schneider, G. Schönhense, Rep. Prog. Phys. **65**, R1785 (2002)
8. W. Kuch, Phys. Scr. T **109**, 89 (2004)
9. J. Vogel, W. Kuch, M. Bonfim, J. Camarero, Y. Pennec, F. Offi, K. Fukumoto, J. Kirschner, A. Fontaine, S. Pizzini, Appl. Phys. Lett. **82**, 2299 (2003)
10. A. Krasyuk, A. Oelsner, S. Nepijko, A. Kuksov, C. Schneider, G. Schonhense, Appl. Phys. A Mater. Sci. Proc. **76**, 863 (2003)
11. C. Schneider, A. Kuksov, A. Krasyuk, A. Oelsner, D. Neeb, S. Nepijko, G. Schonhense, I. Monch, R. Kaltofen, J. Morais, C. de Nadai, N. Brookes, Appl. Phys. Lett. **85**, 2562 (2004)
12. S. Choe, Y. Acremann, A. Scholl, A. Bauer, A. Doran, J. Stöhr, H. Padmore, Science **304**, 420 (2004)
13. J. Raabe, C. Quitmann, C. Back, F. Nolting, S. Johnson, C. Bühler, Phys. Rev. Lett. **94**, 217204 (2005)
14. A. Krasyuk, F. Wegelin, S. Nepijko, H. Elmers, G. Schonhense, M. Bolte, C. Schneider, Phys. Rev. Lett. **95**, 207201 (2005)
15. W. Kuch, J. Vogel, J. Camarero, K. Fukumoto, Y. Pennec, S. Pizzini, M. Bonfim, J. Kirschner, Appl. Phys. Lett. **85**, 440 (2004)
16. J. Vogel, W. Kuch, J. Camarero, K. Fukumoto, Y. Pennec, S. Pizzini, M. Bonfim, F. Petroff, A. Fontaine, J. Kirschner, Phys. Rev. B **71**, 060404 (2005)
17. J. Vogel, W. Kuch, R. Hertel, J. Camarero, K. Fukumoto, F. Romanens, S. Pizzini, M. Bonfim, F. Petroff, A. Fontaine, J. Kirschner, Phys. Rev. B **72**, 220402 (2005)
18. K. Fukumoto, W. Kuch, J. Vogel, F. Romanens, S. Pizzini, J. Camarero, M. Bonfim, J. Kirschner, Phys. Rev. Lett. **96**, 097204 (2006)
19. F. Romanens, J. Vogel, W. Kuch, K. Fukumoto, J. Camarero, S. Pizzini, M. Bonfim, F. Petroff, Phys. Rev. B **74**, 184419 (2006)
20. J. Vogel, W. Kuch, J. Camarero, K. Fukumoto, Y. Pennec, M. Bonfim, S. Pizzini, F. Petroff, A. Fontaine, J. Kirschner, J. Appl. Phys. **95**, 6533 (2004)
21. A. Malozemoff, J. Slonczewski, *Magnetic Domain Walls in Bubble Materials* (Academic, New York, 1979)
22. E. Stoner, E. Wohlfarth, Philos. Trans. Lond. Ser. A **240**, 599 (1948)
23. J. Vogel, J. Moritz, O. Fruchart, C. R. Phys. **7**, 977 (2006)
24. M. Sussiau, F. Nguyen Van Dau, P. Galtier, A. Encinas, A. Schuhl, J. Magn. Magn. Mater. **165**, 1 (1997)
25. F. Montaigne, P. Gogol, J. Briatico, J.L. Maurice, F. Nguyen Van Dau, F. Petroff, A. Fert, A. Schuhl, Appl. Phys. Lett. **76**, 3286 (2000)
26. A. Encinas-Oropesa, F. Nguyen Van Dau, J. Magn. Magn. Mater. **256**, 301 (2003)
27. Y. Pennec, J. Camarero, J.C. Toussaint, S. Pizzini, M. Bonfim, F. Petroff, W. Kuch, F. Offi, K. Fukumoto, F. Nguyen Van Dau, J. Vogel, Phys. Rev. B **69**, 180402 (2004)
28. J. Ferré, *Spin Dynamics in Confined Magnetic Structures I* (Springer, New York, 2002)
29. M. Pierce, C. Buechler, L. Sorensen, J. Turner, S. Kevan, E. Jagla, J. Deutsch, T. Mai, O. Narayan, J. Davies, K. Liu, J. Hunter Dunn, K. Chesnel, J. Kortright, O. Hellwig, E. Fullerton, Phys. Rev. Lett. **94**, 017202 (2005)
30. F. Romanens, S. Pizzini, F. Yokaichiya, M. Bonfim, Y. Pennec, J. Camarero, J. Vogel, J. Sort, F. Garcia, B. Rodmacq, B. Dieny, Phys. Rev. B **72**, 134410 (2005)
31. N. Schryer, L. Walker, J. Appl. Phys. **45**, 5406 (1974)
32. M. Hayashi, L. Thomas, C. Rettner, R. Moriya, S. Parkin, Nat. Phys. **3**, 21 (2007)
33. Y. Nakatani, A. Thiaville, J. Miltat, Nat. Mater. **2**, 521 (2003)
34. A. Mougin, M. Cormier, J. Adam, P. Metaxas, J. Ferré, Europhys. Lett. **78**, 57007 (2007)
35. A. Hubert, R. Schäfer, *Magnetic Domains: The Analysis of Magnetic Microstructures* (Springer, Berlin, 1998)
36. J. Vogel, S. Cherifi, S. Pizzini, F. Romanens, J. Camarero, F. Petroff, S. Heun, A. Locatelli, J. Phys. Condens. Matter **19**, 476204 (2007)
37. L. Néel, C. R. Hebd. Seances Acad. Sci. **255**, 1676 (1962)
38. H. Fuller, D. Sullivan, J. Appl. Phys. **33**, 1063 (1962)
39. W. Kuch, L. Chelaru, K. Fukumoto, F. Porrati, F. Offi, M. Kotsugi, J. Kirschner, Phys. Rev. B **67**, 214403 (2003)
40. R. Schäfer, R. Urban, D. Ullmann, H.L. Meyerheim, B. Heinrich, L. Schultz, J. Kirschner, Phys. Rev. B **65**, 14405 (2002)
41. V. Christoph, R. Schäfer, Phys. Rev. B **70**, 214419 (2004)
42. S. Wiebel, J.-P. Jamet, N. Vernier, A. Mougin, J. Ferré, V. Baltz, B. Rodmacq, B. Dieny, Appl. Phys. Lett. **86**, 142502 (2005)
43. R. Fink, M. Weiss, E. Umbach, D. Preikszas, H. Rose, R. Spehr, P. Hartel, W. Engel, R. Degenhardt, R. Wichtendahl, H. Kuhlenbeck, W. Erlebach, K. Ihmann, R. Schlogl, H. Freund, A. Bradshaw, G. Lilienkamp, T. Schmidt, E. Bauer, G. Benner, J. Electron Spectrosc. Related Phenom. **84**, 231 (1997)